QM/MM Modeling of Environmental Effects on Electronic Transitions of the FMO Complex

ARTICLE *in* THE JOURNAL OF PHYSICAL CHEMISTRY B · MARCH 2013

Impact Factor: 3.3 · DOI: 10.1021/jp3109418 · Source: PubMed

THE JOURNAL OF PHYSICAL CHEMISTRY B

Article

pubs.acs.org/JPCB

QM/MM Modeling of Environmental Effects on Electronic Transitions of the FMO Complex

Junkuo Gao,[†] Wu-Jun Shi,[†] Jun Ye,[‡] Xiaoqing Wang,[§] Hajime Hirao,[§] and Yang Zhao*[,†]

[†]Division of Materials Science, Nanyang Technological University, 50 Nanyang Avenue, Singapore 639798

[‡]Institute of High Performance Computing, Agency for Science, Technology and Research, 1 Fusionopolis Way, 16-16 Connexis, Singapore 138632

[§]Division of Chemistry & Biological Chemistry, Nanyang Technological University, 21 Nanyang Link, Singapore 637371

ABSTRACT: The Fenna–Matthews–Oslon (FMO) light harvesting pigment–protein complex in green sulfur bacteria transfers the excitation energy from absorbed sunlight to the reaction center with almost 100% quantum efficiency. The protein-pigment coupling (part of the environmental effects) is believed to play an important role in determining excitation energy transfer pathways. To study the effect of environment on the electronic transitions in the FMO complex, especially by taking into account the newly discovered eighth extra pigment, we have employed hybrid quantum-mechanics/molecular-mechanics (QM/MM) methods in combination with molecular dynamics (MD) simulations. The averaged site energies of individual pigments are calculated using the semiempirical ZINDO/S-CIS method considering the protein residues as atomic point charges along the MD trajectories. The exciton energies are calculated from the site energies and excitonic couplings based on MD simulations. The new eighth pigment displays the largest site energy and contributes mainly to the highest exciton level, which may facilitate transfer of excitation energies from the baseplate to the reaction center. Further, the multimode Brownian oscillator (MBO) model is used to fit the linear absorption spectra of the FMO complex, validating the exciton energies obtained from the QM/MM calculations. Our results indicate that the QM/MM method combined with MD simulations is a powerful tool to model the environmental effects on electronic transitions of light harvesting antenna complexes.

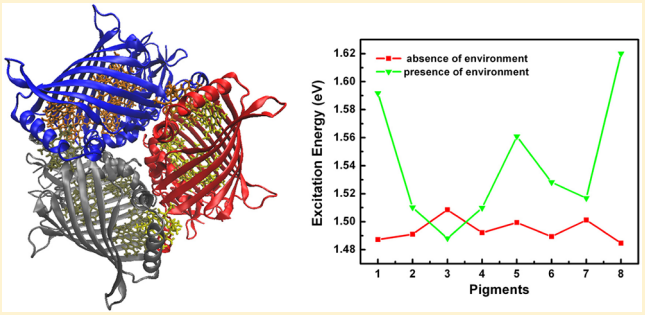

1. INTRODUCTION

Solar to chemical energy conversion in natural photosynthesis is one of the most important biological processes on Earth in which various light harvesting antenna complexes in green plants and photosynthetic bacteria play an important role in harnessing and transferring solar energy to the photosynthetic reaction center (RC) for chemical energy storage.[1−6] The Fenna–Matthews–Olson (FMO) complex in green sulfur bacteria of *Prosthecochloris aestuarii* is the first photosynthetic pigment–protein complex for which an X-ray structure was obtained.[7,8] This FMO complex is embedded in the cytoplasmic membrane and serves as the energy transfer funnel from the chlorosomes to RC complexes. Due to its relatively simple structure among the light harvesting complexes and water solubility, the FMO complex has become one of the most widely studied and well-characterized pigment–protein complexes.[9−13] The FMO complex is a homotrimer containing eight interacting bacterio-chlorophyll a (BChl a) molecules per monomer (Figure 1). The existence of an eighth BChl a molecule in the monomer structure has only recently been discovered,[14−16] while most of the earlier studies had taken into account only seven BChls a. Figure 1b shows the structure of an FMO monomeric unit with the chlorophyll molecules labeled from 1 to 8. Tronrud et al. reported the 1.3 Å resolution structure of the FMO complex from *Prosthecochloris aestuarii* (one of the most studied FMO complex in bacterial species),[15] and it was revealed that the new eighth BChl a is located in one of the clefts on the protein surface of the trimer. Recent chemical labeling and mass spectrometry data determined the orientation of FMO protein on the membrane.[17] It was confirmed that the C_3 symmetry axis of FMO trimer is perpendicular to the membrane, and BChl a 3 is closest to the membrane and serves as the energy sink to the RC complex as predicted by calculations.[18−20] BChls a 1, 6, and 8 are relatively closer to the chlorosome baseplate.[17,21] The location and orientation of BChl a 8 may facilitate energy transfer from the chlorosome baseplate to the RC complex, yet precise assessment of its role has not received adequate attention so far.[22−24]

Site energies of BChl a molecules in the FMO complex are defined as the HOMO to LUMO excitation energy (Q_y state) when the coupling between the pigments is not considered. Site energies are needed for modeling linear spectra and simulating exciton transfer dynamics. Different studies employing optical

Received: November 5, 2012
Revised: March 8, 2013

   dx.doi.org/10.1021/jp3109418 | *J. Phys. Chem. B* XXXX, XXX, XXX–XXX

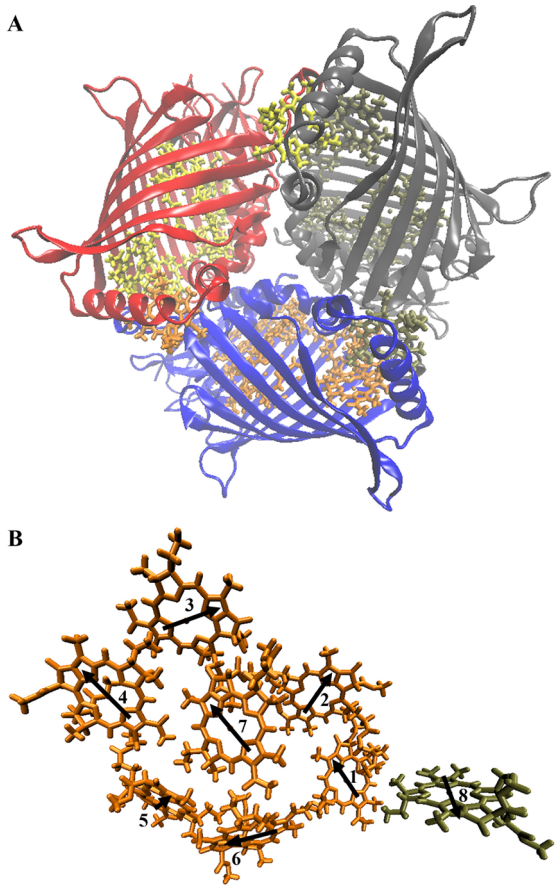

Figure 1. (a) Depiction of the bottom up view of the FMO trimer of *Prosthecochloris aestuarii* including the protein backbone. (b) The BChls a in an FMO monomer where the eighth BChl a is nearby the neighboring monomer. The arrows in panel (b) are the directions of transition dipole moments. Figure drawn using VMD.[31]

spectral fittings and quantum chemistry calculations have yielded quite varying values of site energies of BChl a molecules in the FMO complex.[25−28] Both experimental and theoretical studies revealed that BChl a 3 possesses the lowest site energy.[19,23,29] However, the assignment of the BChl a molecule that has the highest site energy and transfers the energy from the chlorosome is still contentious. Since the presence of the eighth BChl a in FMO monomer was discovered only recently, only two values of its site energy have been reported so far. Study of the FMO protein of *Prosthecochloris aestuarii* by Busch et al., using the combined quantum chemistry and electrostatic calculations, proposed that BChl a 8 exhibits the highest site energy and acts as the linker to the baseplate.[23] They pointed out that this new BChl a plays a very important role by which the large energy gap between BChl a 8 and the sink of BChl a 3 leads to efficient unidirectional energy transfer toward the RC complexes. Olbrich et al. calculated the FMO site energies of *Chlorobaculum tedium* species using a combination of semiempirical quantum chemistry calculations and classical molecular dynamics (MD) simulations. In their studies, BChl a 7 at the middle of the FMO monomer was assigned the highest site energy, while the site energy of BChl a 8 was found close to that of BChl a 1 and BChl a 6.[30] The BChl a 8 molecule forms a bidentate interaction with the protein in the new high resolution crystal structure of FMO *Prosthecochloris aestuarii*. The carbonyl oxygen of residue 123 (Tyrosine) binds to the central magnesium atom on one side, while the O_y atom of residue 168 (Serine) from the nearby monomer is linked to its other side, as shown in Figure 2. In contrast, in the FMO protein of *Chlorobaculum tedium*, only one Tyrosine residue is bonded to BChl a 8. Tronrud et al. claimed that the different binding modes of BChl a 8 molecule in the two species lead to the different absorption spectra at low temperature.[15] Further experimental and theoretical studies are needed to investigate how and to what extent, the BChl a 8 molecule influences the absorption spectra and the excitation energy transfer process.

In this study, we have used a combination of classical MD simulations and semiempirical quantum chemistry methods to

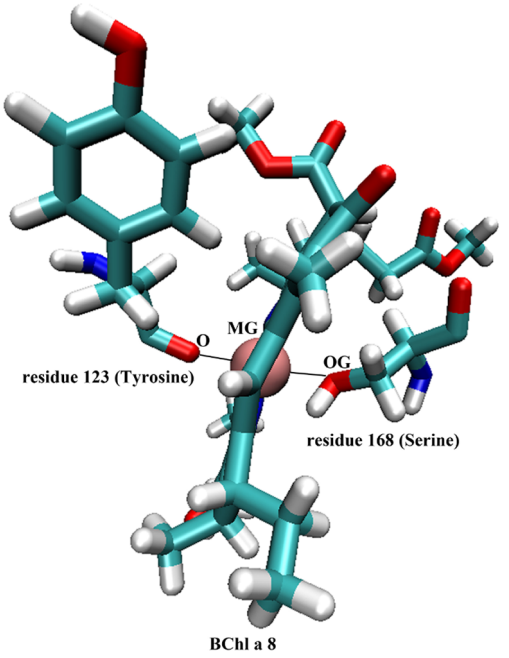

Figure 2. The binding of the eighth BChl a in FMO protein of *Prosthecochloris aestuarii*. Atoms are labeled according the PDB file information. Mg, O, N, C, and H atoms are shown in purple, red, blue, green, and white.

investigate how the protein environment influences site energies and excitation energy transfer in the FMO protein. The new high-resolution structure of *Prosthecochloris aestuarii* was used for our computational modeling. In the semiempirical calculations, the hybrid quantum mechanics/molecular mechanics (QM/MM) approach was employed with the effect of point charges from amino-acid residues on the excitation energies of pigments also taken into account. The role of BChl a 8 in the energy transfer process is discussed based on the QM/MM results. Furthermore, the linear absorption spectra of the FMO trimer are modeled using the multimode Brownian oscillator (MBO) model to validate the exciton energies derived from the QM/MM results.

The rest of the paper is organized as follows. Section 2 describes the details of computational methods used. Results from MD simulations and QM/MM studies are presented and discussed in Section 3.1, whereas details of the MBO model and correspondingly obtained absorption spectrum of the FMO complex are presented in Section 3.2. Finally, Section 4 delineates the conclusions.

dx.doi.org/10.1021/jp3109418 | J. Phys. Chem. B XXXX, XXX, XXX−XXX

2. COMPUTATIONAL DETAILS

MD simulations have been performed on the basis of the trimeric crystal structure of *Prosthecochloris aestuarii* (PDB code: 3eoj) with 8 BChls a per monomer reported by Tronrud et al. at 1.3 Å resolution.[15] The FMO trimer was built using symmetry transformations of the 3eoj structure file. All atoms in the protein scaffold, the BChls a and the water molecules are included in the MD simulation. The pigment−protein complex is embedded in a water box such that there is about 15 Å distance from the boundaries of each complex to the edge of the box. The size of the water box used is 120 × 122 × 93 Å for the system. Equal amounts of sodium and chloride ions were added to simulate the 1.15 mol/L salt concentration. The total atom count is 123 514, and the number of Na^+ and Cl^- ions in the simulation system is 98 and 98 each. The NAMD package is used to perform the MD simulations using the CHARMM27 force field.[32−34] The force field parameters for BChl a are adopted from the literature.[35] The TIP3P model was used for water molecules, while the O−H distances and H−O−H angle of water molecules were constrained using the SHAKE algorithm.[36] The Particle Mesh Ewald (PME) method[37] was used for electrostatic summations while the periodic boundary conditions were employed. Both the electrostatic and the Lennard−Jones interactions had a twin-range cutoff of 10/12 Å. After energy minimization, the system was equilibrated for 10 ns at 300 K and 1 atm pressure, in an NPT ensemble. The time step of integration was 1 fs. The root-mean-square deviation (RMSD) values of the protein backbone and pigments have been calculated to verify the equilibration of the system. The equilibrated structure is then used for MD simulations over further 200 ps. During this production run, atomic coordinates are extracted every 5 fs to subsequently calculate site energies via semiempirical QM calculations.

The site energies associated with the Q_y excitations of all the BChls a in the complex were calculated individually by QM/MM calculations. For this purpose, we utilize the semiempirical Zerner Intermediate Neglect of Differential Orbital method with parameters for spectroscopic properties (ZINDO/S) combined with the Configuration Interaction Singles method (ZINDO/S-CIS), as implemented in ORCA program version 2.8.[38] ZINDO/S-CIS is widely employed in electronic-structure studies of light-harvesting protein systems, providing balanced accuracy and efficiency. To improve the efficiency of QM calculations, the phytyl tail was replaced by a CH_3 group as little influence on the site energies of pigments in light harvesting complex was observed after the replacement. The configuration interaction description using the 10 highest occupied and the 10 lowest unoccupied orbitals was applied, which has earlier been shown to provide a good compromise between efficiency and accuracy.[30,39,40] The protein environment around each BChl a from the MD simulations was treated as atomic point charges within a cutoff radius of 20 Å around the truncated BChl a molecule when calculating the electronic transitions, as this approach is known to provide sufficient accuracy for the QM/MM simulation.[41] Consequently, one can account for the influence of local protein environment on orbital energies. The individual excitation energies of each BChl a were averaged over 40000 snapshots along the MD trajectories.

3. RESULTS AND DISCUSSION

3.1. Calculation of Site Energies and Excitonic Couplings. The MD trajectory for the production run of 200 ps duration begins at the end of equilibration period, and is composed of 40 000 snapshots. The atomic coordinates in each frame are then used for the QM/MM electronic-structure calculations of BChls a in the FMO trimer. Electronic excitations of BChls a are influenced by nuclear dynamics of the pigment−protein complex. Calculations of the excitation energies and excitonic couplings along the MD trajectories are performed to take into account the influence of the thermal fluctuations. To evaluate how the protein environment affects the excitation energies of the BChls a, the local environments including protein residues and other BChls a surrounding an individual BChl a are modeled as point charges in the QM/MM calculations. Ab-initio methods are computationally too expensive for the QM/MM calculations when combined with the MD simulations. Therefore, in the QM/MM treatment, the BChl a molecules are described by the semiempirical ZINDO/S-CIS, while the CHARMM27 force field is used to capture the environmental influence around an individual BChl a. The site energies of the BChls a are first calculated for the FMO trimer containing 8 pigments per monomer, and are shown in Figure 3. To study how the protein environment influences the site

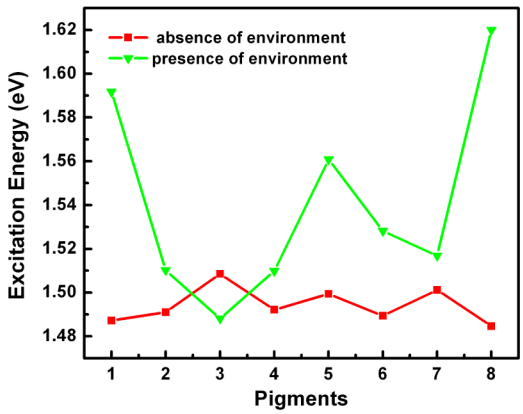

Figure 3. The calculated averaged site energies for individual BChls a in the FMO trimer in the presence (green line) and absence (red line) of the local environment that includes protein residues and other BChls a.

energies, the excitation energies in the absence of the environmental point charges are also calculated. In the absence of the protein environment, BChl a 3 yielded the highest site energy while BChl 8 showed the lowest, and the difference between them is only 24 meV. In this case, the differences in the shifts in site energies of different BChls a can be attributed mainly to the initial geometries of BChls a in the crystal structure. These values contradict the energy flow from chlorosome to RC complex based on the experimental and theoretical calculations. When the point charges of the protein environment are included in the ZINDO QM/MM calculations, the site energies show an obvious change. The atomic point charge distribution of the surrounding local environment generates changes in electrostatic interactions on BChls a, which result in even site-energy shifts of BChls a.[42] The site energy of BChl a 3 is red-shifted by 20 meV and ends up as the lowest values among all the BChls a. This observation is in agreement with that by Müh et al., who in his work, using the combined quantum chemical and electrostatic approach, reported that the α-helices near the BChl a 3 efficiently reduced its site energy to cause it to act as an energy sink.[43]

dx.doi.org/10.1021/jp3109418 | J. Phys. Chem. B XXXX, XXX, XXX−XXX

The site energy of BChl a 8 exhibits quite a large blue shift of 135 meV upon introduction of the environment that includes protein residues and other BChls a and becomes the highest. This is consistent with the general argument that BChl a 8 being attached to the chlorosome baseplate may receive the excitation energy directly from the baseplate. Another large protein-induced blue shift of 104 meV in the site energy is found for BChl a 1. For all of the remaining BChls a, blue shifts in the range of 18∼60 meV are observed. The calculated site energies of FMO trimer were compared with the values calculated by Louwe et al.[18] and Busch et al.[23] for the same bacterium, *Prosthecochloris aestuarii*, and also the results for bacterium of *Chlorobaculum tedium* by Olbrich et al.,[30] as shown in Figure 4. The site energies calculated from fitting of

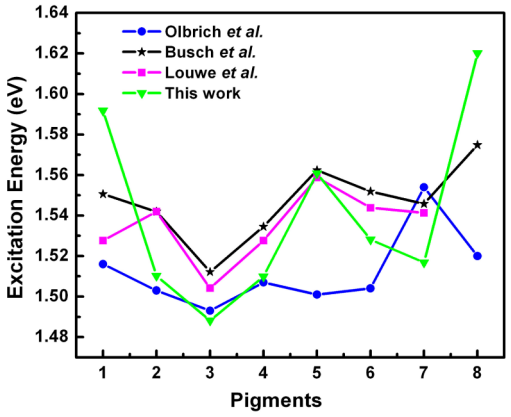

Figure 4. Comparison of individual site energies obtained in the current work (green triangles) with the results from Olbrich et al.[30] (blue circles), Busch et al.[23] (black stars), and Louwe et al.[18] (purple squares).

optical spectra by Louwe et al. correspond to the FMO complex containing seven pigments per monomer, whereas the results by Busch et al. stand as the first evaluation of the site energies in an FMO trimer with the eighth BChls a accounted for in the calculations using the combined quantum and electrostatic approach. It can be seen that the present values show a similar trend as that reported by Busch et al. In order to calculate site energies, Louwe et al. use spectral fitting (squares), and in their work, the lowest (highest) site-energy is found on Bchl a 3 (5). Effect of the local protein environment on electronic transitions of the FMO complex was not included in their study since the pigment−protein couplings were not taken into account. Information from the initial crystal structure is combined with quantum chemical and electrostatic calculations by Busch et al. to determine site energies (stars). Among their results, the highest site energy is found on BChl a 8 with the rest of Bchls having similar energies as those reported by Louwe et al. Olbrich et al. calculated the site energies of the FMO complex in the *Chlorobaculum tedium* species using the semiempirical QM combined with classical MD simulations (circles) with results showing that BChl a 7 has the highest site energy instead of BChl a 8. The only important difference between the current and previous results is in the precise values of site energies. The site energy for BChl a 5 is nearly the same when compared with those of Louwe et al. and Busch et al. For BChl a 1 and BChl a 8, the site energies are higher than the reported values, while for other BChls a the values are lower. There is significantly positive excitonic coupling between BChls a 1 and 8, leading to formation of an H-aggregate between these two BChls a. Therefore, higher excitation energies for these two pigments is a natural consequence of their H-aggregation. The site energy of BChl a 1 is thus higher than that of BChl a 2, in qualitative agreement with the results by Busch's et al. An opposite trend can be seen in the results by Louwe et al. as BChl a 8 was not included therein. It should be noted that different calculation methods could provide different site energies, which are surrounded by contention in the absence of more direct experimental evidence on the excitation energies of individual BChls a in the FMO complex, and could be validated via the modeling of optical spectra.

The excitonic couplings (V_{km}, cm^{-1}) between the transition dipoles of the kth and mth BChl a molecules, assumed as dipolar couplings, are calculated with the point dipole approximation:

$$V_{km} = f\frac{\mu_k\mu_m}{R_{km}^3}[\hat{\mu}_k\cdot\hat{\mu}_m - 3(\hat{\mu}_k\cdot\hat{n}_{km})(\hat{\mu}_m\cdot\hat{n}_{km})] \quad (1)$$

where μ_k (μ_m) is the dipole strength of the Q_y transition (in D) of the kth (mth) BChl a with the direction $\hat{\mu}_k$ ($\hat{\mu}_m$), R_{km} is the distance (in nm) between the dipoles with the direction $\hat{n}_{km}$, and f is a factor that accounts for the dielectric environment (protein screening). The excitonic couplings were calculated and averaged for all snapshots from the MD simulations. In the calculations, the direction of the Q_y transition dipole moment was taken from ND to NB according to the nomenclature of the Protein Data Bank. R_{km} was taken as the distance between the Mg atoms of BChl a k and m. The value of dipole strength $\mu_k\mu_m$ = 37.5 D^2, and the protein screening factor f = 0.8 as reported by Adolphs.[12] With the eighth BChl a of one monomer being closer to BChl a 1 in the adjacent monomer, the excitonic coupling between them is larger than that between the BChl a 8 and any other BChl a from the same monomer that is defined in the crystal structure. Thus to simplify analysis, as shown in Figure 5, we denote a new monomeric unit formed

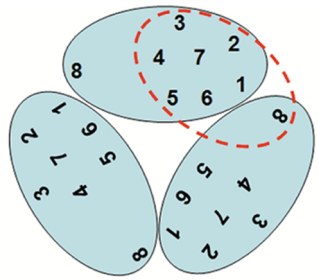

Figure 5. Schematic illustration of the FMO trimer complex. The shaded ovals represent the monomers defined in the crystal structure, while the oval marked with dashed, red boundary represents a monomeric unit defined in this work.

by BChls 1−7 from a given monomer defined in the crystal structure, but with BChl a 8 from the neighboring monomer. The values of excitonic couplings are averaged along the MD trajectories and tabulated in Table 1. The interactions between BChls a in the FMO complex are weak due to the large distances between them (typically, >10 Å). BChl a 1 and BChl a 2 displays the strongest interaction which is −87.6 cm^{-1}. The excitonic coupling between Bchl a 4 and BChl a 5 is −83.6 cm^{-1}, while BChl a 5 also displays strong coupling with BChl a 6 (76.0 cm^{-1}). The eighth BChl a molecule shows strongest

dx.doi.org/10.1021/jp3109418 | J. Phys. Chem. B XXXX, XXX, XXX−XXX

Table 1. Calculated Excitonic Couplings of the FMO Protein in Units of cm^{-1} from the Average of MD Simulation

BChl a	1	2	3	4	5	6	7	8
1	0.0	−87.6	4.3	−6.9	6.7	−20.7	−11.8	27.8
2	−87.6	0	29.4	8.4	1.2	13.4	−1.0	4.0
3	4.3	29.4	0.0	−48.8	−6.9	−10.6	3.0	0.2
4	−6.9	8.4	−48.8	0.0	−83.6	−17.1	−58.9	−1.4
5	6.7	1.2	−6.9	−83.6	0.0	76.0	5.2	3.4
6	−20.7	13.4	−10.6	−17.1	76.0	0.0	52.2	−7.8
7	−11.8	−1.0	3.0	−58.9	5.2	52.2	0.0	−10.9
8	27.8	4.0	0.2	−1.4	3.4	−7.8	−10.9	0.0

Table 2. Exciton Energies (eV) and Exciton Coefficients of the Eigenvectors of the FMO Protein

exciton level	exciton energies	Bchl a 1	Bchl a 2	Bchl a 3	Bchl a 4	Bchl a 5	Bchl a 6	Bchl a 7	Bchl a 8
1	1.485	−0.02	−0.16	**0.94**	0.30	0.03	0.03	0.06	0.001
2	1.505	0.02	0.08	0.27	**0.75**	0.13	−0.11	**0.57**	0.005
3	1.509	0.14	**0.97**	0.18	−0.006	0.001	−0.04	−0.05	−0.02
4	1.520	−0.008	−0.01	0.15	**-0.53**	0.04	**-0.50**	**-0.66**	0.002
5	1.527	0.04	0.05	0.02	−0.19	−0.29	**0.81**	**0.47**	0.02
6	1.565	−0.01	0.01	0.008	−0.15	**0.94**	0.29	0.03	−0.002
7	1.593	**0.98**	−0.14	0.002	0.01	0.02	−0.02	−0.01	−0.16
8	1.621	0.16	−0.01	0.002	−0.002	0.01	−0.01	−0.02	**0.99**

excitonic coupling of 27.9 cm^{-1} with BChl a 1 from the neighboring pigment. The strong coupling between BChl a 1 and BChl a 8 opens up a channel for the excitation energy to enter from the baseplate. For other BChl a molecules within the same pigment, the values of excitonic couplings with BChl a 8 smaller than 11 cm^{-1} denote significantly weak interactions.

The electronic Hamiltonian of the FMO complex can be described as follows:

$$H_0 = \sum_m E_m |m\rangle\langle m| + \sum_{m\neq n} V_{mn} |m\rangle\langle n| \tag{2}$$

where E_m represent the site energies of pigments and $|m\rangle$ the corresponding localized excited states. The delocalized exciton states $|M\rangle$ can be defined as the linear combination of localized excited states

$$|M\rangle = \sum_m c_m^{(M)} |m\rangle \tag{3}$$

wherein the exciton expansion coefficients $c_m^{(M)}$ represent the contribution of the individual BChl a molecules. The eigenvalues and $c_m^{(M)}$ can be calculated by diagonalizing the Hamiltonian and are tabulated in Table 2.

From Table 2 it can be seen that almost all of the exciton states showed some degree of delocalization over several BChl a pigments. BChl a 3 and BChl a 4 dominate the lowest exciton level with some contribution from Bchl a 2. Both exciton levels 2 and 4 are mainly constituted of the excited states of BChl a 3, 4, 6, and 7. The highest exciton level 8 is mainly localized on BChl a 8 which may thus play an important role in transferring energy from the baseplate to the RC complex.

3.2. Linear Optical Spectra Modeling Using the MBO Model. To further support the exciton energies calculated in this work, we employ the multimode Brownian oscillator (MBO) model to fit the linear absorption spectrum of the FMO protein. A detailed description of the MBO model is given in Appendix A. Important parameters for the MBO model include the primary phonon frequency ω_1, the coupling strength between this phonon mode and the optical transition represented by the Huang−Rhys factor S, as well as corresponding damping strength γ of this phonon mode. By introducing the MBO model, we are able to take into account effects of the dissipative environment on the optical process. In our previous studies of polymers, it has been shown that there may exist additional low frequency phonon modes (such as one with ω_2) that couple strongly to excitation.[44] We have adopted a similar approach in this work to reach a satisfactory fitting of the measured spectra so that better comparisons can be made with those obtained from QM/MM calculations.

The best combination of relative intensities of peaks and different exciton energies is achieved via the least mean square error method in conjunction with the MBO model. In the calculation of the absorption spectrum, we have assumed independent transitions for all excitons. Therefore, contributions from the individual spectrum of each exciton level have been combined. Furthermore, the parameters of the MBO spectrum are tuned manually. After obtaining the MBO-derived spectrum for each exciton, the relative intensities and exciton energies are optimized simultaneously till the least mean square error is reached. The results are finally found to be in reasonable agreement with measurements,[15] as clearly demonstrated in Figure 6. The parameters used for fitting are given in Table 3. It can be observed from Figure 6 and Table 3 that the exciton energies obtained through optical spectrum fitting (E_{MBO}) agree well with the ones obtained though QM/MM calculations ($E_{QM/MM}$), with the largest difference well within 0.01 eV. In other words, the maximum difference is less than 1%, therefore lending strong support to the exciton energies obtained from the QM/MM calculations. It is also of interest to analyze the role of phonons in determining spectral features. It can be inferred from our fitting that the contribution of the high frequency phonon mode weakly coupled to excitons leads to the spectral line shape around 1.7 eV. The low frequency mode (ω_2) with stronger coupling to excitons adds further broadening to the spectrum. It is also revealed in Figure 6 that the spectral fitting can be further improved if additional MBO parameters are introduced, or more low-frequency modes are included, therefore increasing the sophistication of the MBO model. For example, it is highly possible that for different

dx.doi.org/10.1021/jp3109418 | J. Phys. Chem. B XXXX, XXX, XXX−XXX

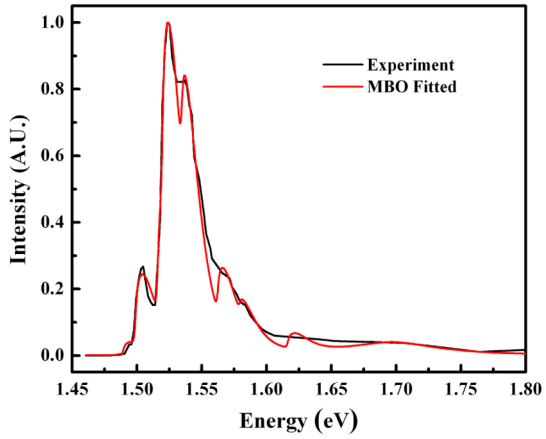

Figure 6. Linear absorption spectra of FMO of *Prosthecochloris aestuarii* fitted by the MBO model combined with the least mean square error method. The parameters obtained through the fitting are given in Table 3. Experimental data are obtained from ref 15.

Table 3. Fitting Parameters for Obtaining Best Fit of Absorption Spectrum of FMO Shown in Appendix A[a]

exciton level	E_{MBO} (eV)	$E_{QM/MM}$ (eV)	$E_{MBO} - E_{QM/MM}$ (eV)	relative intensity
1	1.490	1.485	0.005	0.046
2	1.500	1.505	−0.005	0.252
3	1.518	1.509	−0.009	0.452
4	1.522	1.520	0.002	0.659
5	1.538	1.527	0.011	0.461
6	1.566	1.565	0.001	0.200
7	1.584	1.593	−0.009	0.072
8	1.622	1.621	0.001	0.054
MBO parameters: ω_1 = 1440 cm^{-1}	ω_2 = 106 cm^{-1}	γ_1 = 450 cm^{-1}	γ_2 = 200 cm^{-1}	$S1$ = 0.1, $S2$ = 1.06, T = 6 K

[a]The exciton energies obtained in Table 2 have also been included for comparison.

excitons, excited-state geometries may be very different, leading to considerable changes in their potential energy surfaces and large variations in the exciton−phonon couplings. We only retain one low-frequency mode and one high-frequency mode here. Despite its simplicity, the MBO fitting is still expected to shed light on the role of exciton−phonon coupling in shaping the optical process, and consequently, excitonic energy transfer, in FMO complex.

Besides the reasonable success of the MBO model in fitting exciton energies for the FMO complex in *Prosthecochloris aestuarii*, it is also beneficial to look into the phonon frequencies and their Huang−Rhys factors S obtained from the fitting. From spectral fittings in refs 19 and 45, the overall S obtained for FMO in *Prosthecochloris aestuarii* equals to 0.45, and the frequencies of the phonon modes coupled to excitons are 36, 70, and 195 cm^{-1}. It is interesting to observe the frequency proximity between those modes from refs 19 and 45 and the low-frequency mode of 106 cm^{-1} obtained from our fitting. Furthermore, our MBO analysis also points to the existence of a high-frequency phonon mode (∼1440 cm^{-1}), which was not found in refs 19 and 45. In our fitting, good agreement with the measured line-shape around 1.7 eV can only be obtained by including a high-frequency phonon mode. It should be noted that phonon modes uncovered from the MBO model are regarded as effective modes, and as such, a direct comparison between the MBO results with those from refs 19 and 45 may not be very meaningful. Interestingly, similar low and high frequency modes are found in ref 46, despite that the FMO complex used in the study was from a different species *Chlorobaculum tedium*.

4. CONCLUSIONS

In summary, we have studied the effects of the environment on the electronic transitions of the FMO complex of *Prosthecochloris aestuarii* containing eight Bchls a per monomer via a combination of MD simulations and QM/MM calculations. The site energies are calculated and averaged using the ZINDO/S-CIS method including the surrounding residues as atomic point charges along the MD trajectories. The calculated site energies display a trend similar to the previously published results. The eighth pigment that is closest to the baseplate possesses the largest site energy and may thus be important in transferring energy from the baseplate to the RC complex. The exciton energies are also calculated based on the obtained site energies and excitonic couplings. The use of MBO model to satisfactorily fit the linear absorption spectra of the FMO complex and the good agreement of exciton energy values between both the approaches lends further support to the exciton energies obtained from the QM/MM calculations. These results reveal that the protein environment has substantial influence on the electronic transitions of the FMO complex and the excitonic energy transfer. The QM/MM method combined with MD simulations is thus rendered a powerful tool to model the environmental effects on electronic transitions of light harvesting antenna complexes.

APPENDIX A: LINEAR OPTICAL ABSORPTION SPECTRUM CALCULATIONS

To calculate the linear optical spectrum of the FMO complex, it is essential to know the site energies, excitonic couplings and the optical line width. Different protein environments surrounding BChl a molecules and the dynamic disorder of the FMO complex may cause the optical spectrum to broaden, as a result of the coupling between the electronic transitions, and vibrations of the pigments and their environment (phonons). Using the above site energies and excitonic couplings calculated for FMO trimer, the linear optical spectra could be simulated using the MBO model. The MBO model can be used to study the interactions between electronic and vibrational transitions. It describes the electronic relaxation of a two level system attached to a few primary oscillators which are coupled with a bath of secondary phonons. In the Brownian oscillator model, the Hamitonian is given by[47,48]

$$H = |g\rangle H_g \langle g| + |e\rangle H_e \langle e| + H' \tag{A1}$$

where,

$$H_g = \sum_j \left[\frac{p_j^2}{2m_j} + \frac{1}{2} m_j \omega_j^2 q_j^2 \right] \tag{A2}$$

$$H_e = \hbar\omega_{eg} + \sum_j \left[\frac{p_j^2}{2m_j} + \frac{1}{2} m_j \omega_j^2 (q_j + d_j)^2 \right] \tag{A3}$$

and

dx.doi.org/10.1021/jp3109418 | J. Phys. Chem. B XXXX, XXX, XXX−XXX

$$H' = \sum_n \left[\frac{p_n^2}{2m_n} + \frac{1}{2} m_n \omega_n^2 \left(q_k - \sum^2 \frac{c_{nj} q_j}{m_n \omega_n^2} \right) \right] \tag{A4}$$

In eqs A1−A4, ω_j, p_j, q_j, and m_j is the angular frequency, momentum, coordinate and mass of the primary oscillators for mode j, respectively, d_j is the displacement of the jth nuclear mode in the electronic excited state and $\hbar\omega_{eg}$ is the energy difference in the two-level system. H' represents the coupling between the primary oscillators and bath modes with a coupling strength of c_{nj}. The energy gap operator may be defined as follows:

$$U = H_e - H_g - \hbar\omega_{eg}^0 \tag{A5}$$

The correlation function in the time domain for the jth mode can then be written as follows:

$$C_j(t) = -\frac{1}{2\hbar^2}[\langle U(t)U(0\rho_g)\rangle - \langle U(0)U(t)\rho_g\rangle] \tag{A6}$$

where the operator $U(t)$ is the interaction representation of the operator U. ρ_g is the equilibrium ground state vibrational density matrix defined as follows:

$$\rho_g = \frac{|g\rangle\langle g|\exp(-\beta\hat{H}_g)}{Tr[\exp(-\beta\hat{H}_g)]} \tag{A7}$$

where $\beta = 1/k_B T$. Conversion to frequency domain can be achieved via Fourier transform of the correlation function, and its imaginary part known as the spectral density is then given as follows:

$$\tilde{C}_j''(\omega) = \frac{2\lambda_j \omega_j^2 \omega \gamma_j(\omega)}{\omega^2 \gamma_j^2(\omega) + [\omega_j^2 + \omega\Sigma_j(\omega) - \omega^2]^2} \tag{A8}$$

where $\Sigma_j(\omega)$ is the real part of the self-energy and $2\lambda_j$ is the Stokes shift of the jth mode,

$$\lambda_j = \frac{m_j \omega_j^2 d_j^2}{2\hbar} = S_j \hbar\omega_j \tag{A9}$$

where S_j is the dimensionless Huang−Rhys factor describing the exciton−phonon interaction strength.

In this work, we adopt a simple form of the MBO model, therefore, the spectral distribution function $\gamma_j(\omega)$ is assumed to be in its Ohmic limit (i.e., $\gamma_j(\omega)$ = constant). For simplification, we set the self-energy term $\Sigma_j(\omega) = 0$. Under this condition, the spectral density for the jth primary oscillator has the following form:

$$C_j''(\omega) = \frac{2\lambda_j \omega_j^2 \omega \gamma_j}{\omega^2 \gamma_j^2 + (\omega_j^2 - \omega^2)^2} \tag{A10}$$

AUTHOR INFORMATION

Corresponding Author

*Phone: (+65) 6513 7990; e-mail: YZhao@ntu.edu.sg.

Notes

The authors declare no competing financial interest.

ACKNOWLEDGMENTS

The authors thank U. Kleinekathöfer for providing force-field parameters for BChl a pigments in the MD simulation. Support from the Singapore National Research Foundation through the Competitive Research Programme (CRP) under Project No. NRF-CRP5-2009-04 is gratefully acknowledged. H.H. is thankful for the support of an NTU start-up grant.

REFERENCES

(1) Chu, S.; Majumdar, A. Opportunities and Challenges for a Sustainable Energy Future. *Nature* **2012**, *488*, 294−303.

(2) Umena, Y.; Kawakami, K.; Shen, J. R.; Kamiya, N. Crystal Structure of Oxygen-Evolving Photosystem II at a Resolution of 1.9 Å. *Nature* **2011**, *473*, 55−65.

(3) Ahn, T. K.; Avenson, M.; Ballottari, M.; Cheng, Y. C.; Niyogi, K. K.; Bassi, R.; Feeming, G. R. Architecture of a Charge-Transfer State Regulating Light Harvesting in a Plant Antenna Protein. *Science* **2008**, *320*, 794−797.

(4) Scholes, G. D.; Fleming, G. R.; Olaya-Castro, A.; van Grondelle, R. Lessons from Nature About Solar Light Harvesting. *Nat. Chem.* **2011**, *3*, 763−774.

(5) Cheng, Y. C.; Fleming, G. R. Dynamics of Light Harvesting in Photosynthesis. *Annu. Rev. Phys. Chem.* **2009**, *60*, 241−262.

(6) Camara-Artigas, A.; Blankenship, R. E.; Allen, J. P. The Structure of the FMO Protein from Chlorobium Tepidum at 2.2 Å Resolution. *Photosynth. Res.* **2003**, *75*, 49−55.

(7) Fenna, R. E.; Matthews, B. W. Chlorophyll Arrangement in a Bacteriochlorophyll Protein from *Chlorobium limicola*. *Nature* **1975**, *258*, 573−577.

(8) Tronrud, D. E.; Schmid, M. F.; Matthews, B. W. Structure and X-ray Amino Acid Sequence of a Bacteriochlorophyll Protein from Prosthecochloris Aestuarii Refined at 1.9Å Resolution. *J. Mol. Biol.* **1986**, *188*, 443−454.

(9) Kim, H. W; Kelly, A.; Park, J. W.; Rhee, Y. M. All-Atom Semiclassical Dynamics Study of Quantum Coherence in Photosynthetic Fenna−Matthews−Olson Complex. *J. Am. Chem. Soc.* **2012**, *134*, 11640−11651.

(10) Engle, G. S.; Calhoun, T. R.; Read, E. L.; Ahn, T. K.; Manal, T.; Cheng, Y. C.; Blankenship, R. E.; Fleming, G. R. Evidence for Wavelike Energy Transfer through Quantum Coherence in Photosynthetic Systems. *Nature* **2007**, *446*, 782−786.

(11) Pachon, L. A.; Brumer, P. Computational Methodologies and Physical Insights into Electronic Energy Transfer in Photosynthetic Light-Harvesting Complexes. *Phys. Chem. Chem. Phys.* **2012**, *14*, 10094−10108.

(12) Adolphs, J.; Muh, F.; Madjet, M. E. A.; Renger, T. Calculation of Pigment Transition Energies in the FMO Protein. *Photosynth. Res.* **2008**, *95*, 197−209.

(13) Olson, J. M. the FMO Protein. *Photosynth. Res.* **2004**, *80*, 181−187.

(14) Ben-Shem, A.; Frolow, F.; Nelson, N. Evolution of Photosystem I: From Symmetry Through Pseudosymmetry to Asymmetry. *FEBS Lett.* **2004**, *564*, 274−280.

(15) Tronrud, D. E.; Wen, J.; Gay, L.; Blankenship, R. E. The Structural Basis for the Difference in Absorbance Spectra for the FMO Antenna Protein from Various Green Sulfur Bacteria. *Photosynth. Res.* **2009**, *100*, 79−87.

(16) Tronrud, D. E.; Allen, J. P. Reinterpretation of the Electron Density at the Site of the EighthBbacteriochlorophyll in the FMO Protein from Pelodictyon Phaeum. *Photosynth. Res.* **2012**, *112*, 71−74.

(17) Wen, J.; Zhang, H.; Gross, M. L.; Blankenship, R. E. Native Electrospray Mass Spectrometry Reveals the Nature and Stoichiometry of Pigments in the FMO Photosynthetic Antenna Protein. *Biochemisry* **2011**, *50*, 3502−3511.

(18) Louwe, R.; Vrieze, J.; Hoff, A.; Aartsma, T. Toward an Integral Interpretation of the Optical Steady-State Spectra of the FMO-Complex of Prosthecochloris Aestuarii. 2. Exciton Simulations. *J. Phys. Chem. B* **1997**, *101*, 11280−11287.

(19) Wendling, M.; Przyjalgowski, M. A.; Gülen, D.; Vulto, S. I. E.; Aarstma, T.; van Grondelle, R.; van Amerongen, H. The Quantitative Relationship Between Structure and Polarized Spectroscopy in the

FMO Complex of Prosthecochloris Aestuarii: Refining Experiments and Simulations. *Photosynth. Res.* **2002**, *71*, 99−123.
(20) Adolphs, J.; Renger, T. How Proteins Trigger Excitation Energy Transfer in the FMO Complex of Green Sulfur Bacteria. *Biophys. J.* **2006**, *91*, 2778−2797.
(21) Wen, J.; Zhang, H.; Gross, M. L.; Blankenship, R. E. Membrane Orientation of the FMO Antenna Protein from Chlorobaculum Tepidum as Determined by Mass Spectrometry-Based Footprinting. *Proc. Natl. Acad. Sci., U. S. A.* **2009**, *106*, 6134−6139.
(22) Olbrich, C.; Strumpfer, J.; Schulten, K.; Kleinekathofer, U. Theory and Simulation of the Environmental Effects on FMO Electronic Transitions. *J. Phys. Chem. Lett.* **2011**, *2*, 1771−1776.
(23) Busch, M. S. A.; Muh, F.; Madjet, M. E.; Renger, T. The Eighth Bacteriochlorophyll Completes the Excitation Energy Funnel in the FMO Protein. *J. Phys. Chem. Lett.* **2011**, *2*, 93−98.
(24) Muhlbacher, L.; Kleinekathofer, U. Preparational Effects on the Excitation Energy Transfer in the FMO Complex. *J. Phys. Chem. B* **2012**, *116*, 3900−3906.
(25) Milder, M. T. W.; Bruggemann, B.; van Grondelle, R.; Herek, J. L. Revisiting the Optical Properties of the FMO Protein. *Photosynth. Res.* **2010**, *104*, 257−274.
(26) Adolphs, J.; Renger, T.; Muh, F.; Madjet, M. E. A. Theory of Optical Spectra—How Proteins Control Excitation Energy Transfer. *Photosynth. Res.* **2007**, *91*, 161−162.
(27) Vulto, S.; De Baat, M.; Neerken, S.; Nowak, F.; Van Amerongen, H.; Amesz, J.; Aartsma, T. Excited State Dynamics in FMO Antenna Complexes from Photosynthetic Green Sulfur Bacteria: A Kinetic Model. *J. Phys. Chem. B* **1999**, *103*, 8153−8161.
(28) Pearlstein, R. M. Theory of the Optical Spectra of the Bacteriochlorophyll a Antenna Protein Trimer from *Prosthecochloris aestuarii*. *Photosynth. Res.* **1992**, *31*, 213−226.
(29) Read, E. L.; Schlau-Cohen, G. S.; Engel, G. S.; Wen, J.; Blankenship, R. E.; Fleming, G. R. Visualization of Excitonic Structure in the Fenna-Matthews-Olson Photosynthetic Complex by Polarization-Dependent Two-Dimensional Electronic Spectroscopy. *Biophys. J.* **2008**, *95*, 847−856.
(30) Olbrich, C.; Strumpfer, J.; Schulten, K.; Kleinekathofer, U. Quest for Spatially Correlated Fluctuations in the FMO Light-Harvesting Complex. *J. Phys. Chem. B* **2011**, *115*, 758−764.
(31) Humphrey, W.; Dalke, A.; Schulten, K. VMD—Visual Molecular Dynamics. *J. Mol. Graphics* **1996**, *14*, 33−38.
(32) Mackerell, A. D.; Feig, M.; Brooks, C. L. Extending the Treatment of Backbone Energetics in Protein Force Fields: Limitations of Gas-Phase Quantum Mechanics in Reproducing Protein Conformational Distributions in Molecular Dynamics Simulations. *J. Comput. Chem.* **2004**, *25*, 1400−1415.
(33) MacKerell, A. D.; Bashford, D.; Bellott, M.; Dunbrack, R. L.; Evanseck, J. D.; Field, M. J.; Fischer, S.; Gao, J.; Guo, H.; Ha, S.; et al. All-Atom Empirical Potential for Molecular Modeling and Dynamics Studies of Proteins. *J. Phys. Chem. B* **1998**, *102*, 3586−3616.
(34) Phillips, J. C.; Braun, R.; Wang, W.; Gumbart, J.; Tajkhorshid, E.; Villa, E.; Chipot, C.; Skeel, R. D.; Kale, L.; Schulten, K. Scalable Molecular Dynamics With NAMD. *J. Comput. Chem.* **2005**, *26*, 1781−1802.
(35) Damjanovic, A.; Kosztin, I.; Kleinekathofer, U.; Schulten, K. Excitons in a Photosynthetic Light-Harvesting System: A Combined Molecular Dynamics, Quantum Chemistry and Polaron Model Study. *Phys. Rev. E.* **2002**, *65*, 031919.
(36) Ryckaert, J. P.; Ciccotti, G.; Berendsen, H. J. C. Numerical-Integration of Cartesian Equations of Motion of a System with Constraints: Molecular Dynamics of N-Alkanes. *J. Comput. Phys.* **1977**, *23*, 327−341.
(37) Darden, T.; Perera, L.; Li, L. P.; Pedersen, L. New Tricks for Modelers from the Crystallography Toolkit: The Particle Mesh Ewald Algorithm and Its Use in Nucleic Acid Simulations. *Struct. Fold. Des.* **1999**, *7*, R55−R60.
(38) Neese, F. *ORCA. An Ab Initio, Density Functional and Semiempirical Program Package, Version 2.8*; University of Bonn: Bonn, Germany, 2010.
(39) Olbrich, C.; Kleinekathofer, U. From Atomistic Modeling to Excitation Transfer and Two-Dimensional Spectra of the FMO Light-Harvesting Complex. *J. Phys. Chem. B* **2011**, *115*, 8609−8621.
(40) Zwier, M. C.; Shorb, J. M.; Krueger, B. P. Hybrid Molecular Dynamics-Quantum Mechanics Simulations of Solute Spectral Properties in the Condensed Phase: Evaluation of Simulation Parameters. *J. Comput. Chem.* **2007**, *28*, 1572−1581.
(41) Olbrich, C.; Kleinekathofer, U. Time-Dependent Atomistic View on the Electronic Relaxation in Light-Harvesting System II. *J. Phys. Chem. B* **2010**, *114*, 12427−12437.
(42) Vassiliev, S.; Mahboob, A.; Bruce, D. Calculation of Chromophore Excited State Energy Shifts in Response to Molecular Dynamics of Pigment-Protein Complexes. *Photosynth. Res.* **2011**, *110*, 25−38.
(43) Muh, F.; Madjet, M. W. A.; Adolphs, J.; Abdurahman, A.; Rabenstein, B.; Ishikita, H.; Knapp, E. W.; Renger, T. α-Helices Direct Excitation Energy Flow in the Fenna-Matthews-Olson Protein. *Proc. Natl. Acad. Sci., U. S. A.* **2007**, *104*, 16862−16867.
(44) Ye, J.; Grimsdale, A. C.; Zhao, Y. Analyzing the Optical Properties of a Conjugated Polymer by the Multimode Brownian Oscillator Model. *J. Phys. Chem. A* **2010**, *114*, 504−508.
(45) Wendling, M.; Pullerits, T.; Przyjalgowski, M. A.; Vulto, S. I. E.; Aarstma, T.; van Grondelle, R.; van Amerongen, H. Electron-Vibrational Coupling in the Fenna−Matthews−Olson Complex of Prosthecochloris aestuarii Determined by Temperature-Dependent Absorption and Fluorescence Line-Narrowing Measurements. *J. Phys. Chem. B* **2000**, *104*, 5825−5831.
(46) Rätsep, M.; Freiberg, A. Electron-Phonon and Vibronic Couplings in the FMO Bacteriochlorophyll *a* Antenna Complex Studied by Difference Fluorescence Line Narrowing. *J. Lumin.* **2007**, *127*, 251−259.
(47) Zhao, Y.; Knox, R. S. A Brownian Oscillator Approach to the Kennard-Stepanov Relation. *J. Phys. Chem. A* **2000**, *104*, 7751−7761.
(48) Ye, J.; Zhao, Y.; Ng, N.; Cao, J. Width of Phonon Sidebands in the Brownian Oscillator Model. *J. Phys. Chem. B* **2009**, *113*, 5897−5904.